Articles

Catalytic Residues and an Electrostatic Sandwich That Promote Enolpyruvyl Shikimate 3-Phosphate Synthase (AroA) Catalysis[†]

Paul J. Berti*[,‡,§] and Paul Chindemi[‡]

Departments of Chemistry and Biochemistry and Biomedical Sciences, McMaster University, 1280 Main Street West, Hamilton, Ontario, L8S 4M1, Canada

Received December 10, 2008; Revised Manuscript Received March 9, 2009

ABSTRACT: Enolpyruvylshikimate 3-phosphate synthase (EPSP synthase, AroA) catalyzes the sixth step in aromatic amino acid biosynthesis. It forms EPSP from shikimate 3-phosphate (S3P) and phosphoenolpyruvate (PEP) in an addition/elimination reaction that proceeds through a tetrahedral intermediate. In spite of numerous mechanistic studies, the catalytic roles of specific amino acid residues remain an open question. Recent experimental evidence for cationic intermediates or cationic transition states, and a consideration of the catalytic imperative, have guided this study on the catalytic roles of Lys22 (K22), Asp313 (D313), and Glu341 (E341). Steady-state and pre-steady-state kinetics and protein stability studies showed that mutations of D313 and E341 caused k_{cat} to decrease up to 30 000-fold and 76 000-fold, respectively, while the effects on K_M were modest, never more than 40-fold. Thus, both are identified as catalytic residues. In an active site that is overwhelmingly positively charged, the D313 and E341 side chains are positioned to form an "electrostatic sandwich" around the positive charge at C2 in cationic intermediates/transition states, stabilizing them and thereby promoting catalysis. Mutation of K22 showed large effects on $K_{M,S3P}$ (100-fold), $K_{M,PEP}$ (>760-fold), and up to 120-fold on k_{cat}. Thus, K22 had roles in both substrate-binding and transition-state stabilization. These results support the identification of E341 and K22 as general acid/base catalytic residues.

The reaction catalyzed by enolpyruvyl shikimate 3-phosphate synthase (AroA, also called EPSP synthase) has been extensively characterized and >30 crystal structures have been solved; however, the catalytic roles of individual amino acid residues remain an open question. Identifying their roles is essential to understanding how AroA catalyzes its reaction and eventually to designing AroA inhibitors.[1]

AroA is a carboxyvinyl transferase that forms enolpyruvyl shikimate 3-phosphate (EPSP) and phosphate (P_i) from shikimate 3-phosphate (S3P) and phosphoenolpyruvate (PEP) (Figure 1) as part of the shikimate biosynthetic pathway in bacteria, plants, and some parasites (*1, 2*). AroA is a potential antibacterial target, as knockout strains are avirulent (*3, 4*). In plants, it is the target of the herbicide glyphosate (*5*). Its only homologue, MurA, is also a carboxyvinyl transferase and is part of the peptidoglycan biosynthetic pathway in bacteria. It is the target of the antibiotic fosfomycin (*6*).

The AroA and MurA reactions involve an addition step to form a tetrahedral intermediate (THI) followed by an elimination step to form the enolpyruvyl product (*1, 7, 8*). AroA accelerates THI breakdown $>10^5$-fold relative to nonenzymatic breakdown (*9*). We recently showed that AroA is capable of stabilizing the EPSP cation in the active site (Figure 1) (*10*), and that it must activate the enolpyruvyl group for the reaction to occur. It was not possible to distinguish whether the elimination step normally involves a discrete EPSP cationic intermediate or a highly cationic E2 transition state with P_i departure leading deprotonation, but, in either case, a cationic transition state will be formed. For simplicity, we refer to cationic intermediates throughout this report with the understanding that addition and/or elimination may be concerted. Factors that stabilize the putative cationic intermediates will also stabilize concerted, highly cationic transition states. Solvent tritium exchange at PEP C3 in the presence of the substrate analogue 4,5-dideoxyshikimate 3-phosphate indicates that AroA can also stabilize the PEP cation in the addition step (*11*), indicating that both steps require enolpyruvyl activation and proceed through cationic transition states.

[†] This work was supported by the Canadian Institutes of Health Research.

* To whom correspondence should be addressed. Telephone: (905) 525-9140 ext. 23479. Fax: (905) 522-2509. E-mail: berti@mcmaster.ca.

[‡] Department of Chemistry.

[§] Department of Biochemistry and Biomedical Sciences.

[1] Abbreviations: $AroA_{H6}$, EPSP synthase with C-terminal extension terminating with His_6; EPSP, enolpyruvyl shikimate 3-phosphate; EP-UDPGlcNAc, enolpyruvyl uridine diphosphate *N*-acetyl-glucosamine; F-THI, 3-fluoro-derivative of the enzymatic tetrahedral intermediate; MG/AM, Malachite Green/ammonium molybdate assay for phosphate; MurA, EP-UDP-GlcNAc synthase; PEP, phosphoenolpyruvate; P_i, inorganic phosphate; S3P, shikimate 3-phosphate; THI, enzymatic tetrahedral intermediate.

10.1021/bi802251s CCC: $40.75
Published on Web 03/09/2009

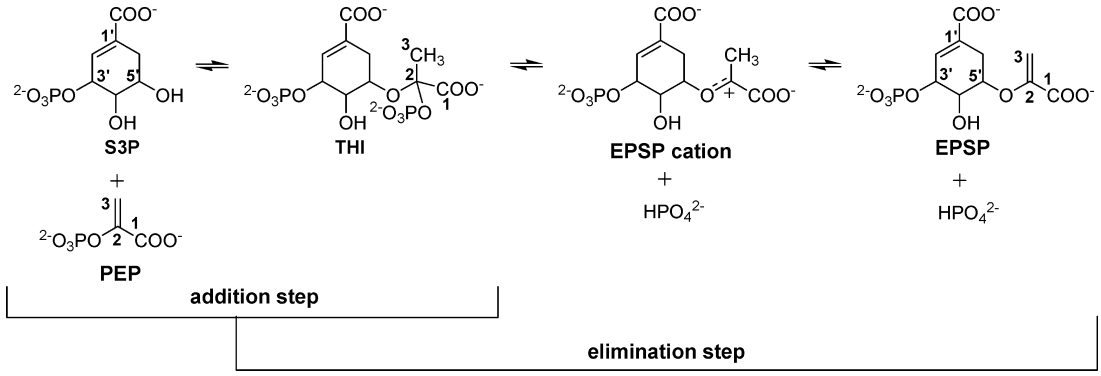

FIGURE 1: The AroA-catalyzed reaction, showing the noncovalent THI and EPSP cationic intermediate.

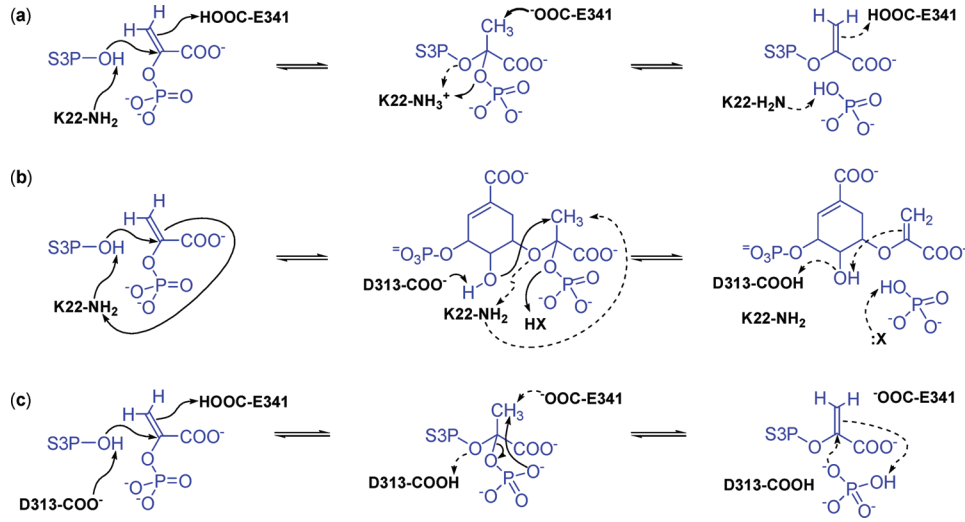

FIGURE 2: Acid−base catalytic residues proposed in various studies. Solid lines represent the forward reaction to EPSP + P_i, dotted lines the reverse reaction, and the thick line indicates a step operating in both forward and reverse reactions. (a) Mizyed et al. (*12*), (b) Eschenburg et al. (*22*), and (c) An et al. (*23*). General base catalysis by D313 was also proposed by Park et al. (*24*).

THI partitioning experiments identified residues K22 and E341 as acid/base catalytic residues (*12*) (Figure 2a). With [1-^{14}C]THI as the substrate, AroA favors the forward reaction to EPSP + P_i over the reverse reaction to S3P + PEP in a ratio of 3:1 (*12, 13*). If a particular amino acid stabilizes the transition state for only the forward reaction, then mutating it will cause THI partitioning to shift completely to the reverse reaction and vice versa. All 18 amino acid side chains within 5 Å of the reactive atoms in the THI were mutated, but none caused significant shifts in partitioning, indicating that the catalytic residues that promote THI breakdown are the same in the forward and reverse reactions. THI partitioning was consistent with either D313 or E341 deprotonating C3, but only E341 would give the correct overall stereochemistry for the reaction (*14*−*19*). This would imply that E341 is also the general acid catalyst that protonates C3 in the addition step. K22 was proposed to deprotonate S3P O5′H in the addition step and to protonate the phosphate bridging oxygen in the elimination step. This is consistent with experimental (*9*) and computational (*20*) studies which show that phosphate elimination is promoted only by protonation of the bridging oxygen, not the nonbridging oxygens. It is also consistent with the experimentally estimated pK_a of 7.6 for K22, 3 pH units below an unperturbed Lys side chain (*21*). This places over half of K22 in the neutral form at physiological pH, as required for K22 to act as a general base in THI formation.

Other mechanisms have been proposed using some combination of K22, D313, and E341 as acid/base catalytic residues. One proposal was based on two remarkable THI-containing crystal structures, AroA(D313A)·THI and the equivalent MurA mutant, MurA(D305A)·THI (*22*). K22 was proposed to be both the acid and base catalyst in the addition step, protonating PEP C3 and deprotonating S3P O5′H (Figure 2b), while D313 was proposed to be the general base catalyst in the elimination step, deprotonating C3 via O4′H (Figure 2b). Other mechanisms have D313 deprotonating S3P O5′H in the addition step (*23, 24*) and E341 protonating C3 (*23*), while substrate-assisted catalysis promotes the elimination step, with phosphate deprotonating C3 (Figure 2c) (*17, 23*).

We have examined mutations to the proposed catalytic residues in light of the competing mechanistic proposals. Some AroA mutations have been reported previously to decrease specific activity (*12, 21, 22, 25*−*32*), but detailed kinetic characterization has generally been lacking. Our steady-state kinetic analysis revealed that K22's greatest contribution is to substrate binding, while D313 and E341 are primarily catalytic residues. This is consistent with E341's proposed role as an acid/base catalyst. In addition, E341 and D313 are proposed to form an "electrostatic sandwich" to stabilize the cationic intermediates of THI formation and breakdown.

EXPERIMENTAL PROCEDURES

Enzymes and Substrates. Recombinant wild-type *Escherichia coli* AroA, His-tagged AroA ($AroA_{H6}$), and AroA mutants were produced as described previously (*12*), except that $AroA_{H6}$

was overexpressed at 18 °C, rather than 37 °C. The active site concentration of $AroA_{H6}$ was determined, as previously, by titration of Trp fluorescence with S3P in the presence of excess glyphosate (*12, 33*). The lower expression temperature caused no change in $AroA_{H6}$'s kinetic constants, but it did result in a higher percentage of active protein after purification, increasing from 40−50% to as high as 80%. Active site titrations with mutant proteins were not successful because of the decreased affinity for S3P and were not routinely performed. Instead, the protein concentration was used for calculating kinetic constants. The modest effects of the mutations on protein stability (see below) suggest that the percentage of active protein would be similar between $AroA_{H6}$ and the mutant proteins. New mutants were produced using the same Quikchange-like strategy as before (*12*). Shikimate 3-phophate (S3P) was produced as described previously (*12*).

Steady State Kinetics. Some reaction rates were determined as described previously using [^{33}P]PEP and ion exchange TLC to detect [^{33}P]P_i formation (*12*). However, this method gave artifactually high rates for low-activity mutants where high protein concentrations were needed, so reaction rates were routinely determined from P_i product formation using the Malachite Green/ammonium molybdate (MG/AM) assay (*34, 35*) in 96 well microtiter plates with 1/2 area wells. MG/AM solution contained 0.063% Malachite Green, 0.1% Tween 20, and 2.1% ammonium molybdate in 2 M HCl. Reactions were started by adding 15−25 μL of reaction buffer containing enzyme and one substrate held at a fixed concentration to an equal volume of reaction buffer containing the variable substrate. Reaction starting times were staggered so that all reactions finished within 10 min of each other, at which time 50 μL of MG/AM solution was added. After 90 s, 10 μL of 34% sodium citrate was added, and A_{660} was measured 30 min later. The assay is nonlinear at very low [P_i], presumably due to incomplete P_i complexation by the MG/AM reagent; thus, K_2HPO_4 (typically ca. 5 μM) was added to the MG/AM solution to ensure that incremental P_i produced by AroA would be in the linear range.

Rates were measured with one substrate concentration held fixed, generally [S3P] = 3 mM or [PEP] = 8 mM. The other substrate concentration was varied from 0.1 to 10 × K_M, though in some cases it was not possible to reach 10 × K_M before contaminating P_i in the S3P or PEP (generally ∼1%) saturated the MG/AM assay. In all cases, there was no P_i formation if either substrate was absent, indicating that the observed activity did not arise from contaminating phosphatases, and that the AroA mutants did not hydrolyze PEP in the absence of S3P.[2] Wild-type AroA reactions were in 50 mM Tris-HCl, pH 7.5, 100 mM KCl, 1 mM EDTA, and 1 mM DTT at 25 °C, as were some $AroA_{H6}$ reactions. Other $AroA_{H6}$ rate assays and all the mutant rate measurements were under the same conditions, except with 50 mM KCl, as noted in the Results section. At least four independent [S] versus $v_0/[E]_0$ profiles were combined when determining the steady-state kinetic constants.

The AroA kinetic mechanism is random sequential with synergistic substrate binding (*36, 37*). In this study, because one substrate was always kept fixed at a high concentration, it was possible to neglect substrate synergism and fit the rate data to eq 1:

$$\frac{v_0}{[E]_0} = \frac{\dfrac{k_{cat}[S3P][PEP]}{K_{M,S3P}K_{M,PEP}}}{1 + \dfrac{[S3P]}{K_{M,S3P}} + \dfrac{[PEP]}{K_{M,PEP}} + \dfrac{[S3P][PEP]}{K_{M,S3P}K_{M,PEP}}} \quad (1)$$

$(k_{cat}/K_M)_{S3P}$ and $(k_{cat}/K_M)_{PEP}$ values were fitted directly to eq 2 rather than from the individual k_{cat} and K_M values.

$$\frac{v_0}{[E]_0} = \frac{\left(\dfrac{k_{cat}}{K_M}\right)_{S3P}\dfrac{[S3P][PEP]}{K_{M,PEP}}}{1 + \dfrac{[S3P]}{K_{M,S3P}} + \dfrac{[PEP]}{K_{M,PEP}} + \dfrac{[S3P][PEP]}{K_{M,S3P}K_{M,PEP}}} \quad (2)$$

Thermal Denaturation. Thermal denaturation of $AroA_{H6}$ was irreversible, so true melting temperatures could not be determined. Using fast heating rates (10 °C/min) to minimize precipitation, apparent melting temperatures were measured from the decrease in intrinsic Trp fluorescence as a function of temperature. $AroA_{H6}$ (1 μM) or mutants in 50 mM Tris-HCl, pH 7.5, 1 mM EDTA, 100 mM KCl, and 1 mM DTT were placed in a fluorescence cuvette and heated from 20 to 80 °C with λ_{ex} = 280 nm and λ_{em} = 338 nm.

Acrylamide Fluorescence Quenching. The solvent accessibility and flexibility of the active site were assessed using acrylamide quenching of the intrinsic Trp fluorescence. Conditions were the same as for thermal denaturation, with spectra collected at 20 °C and 0.5 or 1 μM protein. Aliquots of 10 M acrylamide were titrated into the enzyme solution up to ∼1 M acrylamide. The Stern−Volmer constant, K_{SV}, was determined by fitting the fluorescence versus [acrylamide] data directly to eq 3 (*38*):

$$\frac{F_0}{F} = (1 + K_{SV}[\text{acrylamide}])e^{V[\text{acrylamide}]} \quad (3)$$

where F_0 is the initial fluorescence, F is fluorescence at a given [acrylamide], K_{SV} is the Stern−Volmer constant, the collisional component of quenching, and V is the static quenching component.

Active Site Model. A model of the AroA active site was generated from the *E. coli* AroA(D313A)·THI crystal structure (PDB code: 1Q36) (*22*) and *Streptococcus pneumoniae* AroA·F-THI (1RF4) (*24*) (see Figure 6). The model consists of the THI and side chains from 1Q36, except for

[2] In principle, P_i could have been formed by PEP hydrolysis in the presence of S3P or THI breakdown to {S3P + pyruvate + P_i}. However, previous partitioning studies showed that using [1-^{14}C]THI as a substrate produced [1-^{14}C]PEP and [1-^{14}C]EPSP, but no [1-^{14}C]pyruvate (*12*). This was true for $AroA_{H6}$, K22A, K22R, D313A, D313N, H385A, E341A, and E341Q. If THI breaks down normally, then the principle of microscopic reversibility requires that THI formation must be able to occur in the forward reaction. If mutant AroAs did produce {S3P + pyruvate + P_i} at very low rates instead of {EPSP + P_i}, then it would simply indicate that the normal reaction was even slower than the observed rate and the conclusion that those residues are catalytically important would not be affected. As described below, AroA's main catalytic imperative is to form a PEP cation intermediate or a highly cationic transition state. If a hypothetical mutant stabilized a PEP cation with wild-type efficiency, but used a water nucleophile (forming pyruvate) instead of using S3P (forming EPSP), then the enzyme's catalytic ability would be considered uncompromised and the defect would be in S3P binding or localization. Conversely, to the extent that P_i production is slowed, the mutant enzymes are catalytically compromised even if pyruvate were to be formed.

Table 1: Steady-State Kinetic Parameters for Wild-Type AroA and His_6-Tagged Protein $AroA_{H6}$[a]

	k_{cat} (s^{-1})	$(k_{cat}/K_M)_{S3P}$ ($M^{-1}\cdot s^{-1}$)	$(k_{cat}/K_M)_{PEP}$ ($M^{-1}\cdot s^{-1}$)	$K_{M,S3P}$ (M)	$K_{M,PEP}$ (M)	K_{SV} (M^{-1})
$AroA_{H6}$ (50 mM KCl)	32 ± 1	1.8 (±0.4) × 10^6	8 (±2) × 10^5	1.8 (±0.4) × 10^{-5}	4.0 (±0.9) × 10^{-5}	4.9 ± 0.2
$AroA_{H6}$ (100 mM KCl)	13 ± 1	1.5 (±0.2) × 10^5	9 (±1) × 10^4	1.1 (±0.2) × 10^{-4}	1.5 (±0.3) × 10^{-4}	
AroA (100 mM KCl)	14 ± 1	9.6 (±0.9) × 10^4	8.6 (±0.8) × 10^4	1.4 (±0.2) × 10^{-4}	1.6 (±0.2) × 10^{-4}	

[a] Reactions were performed in 50 mM Tris-HCl, pH 7.5, 1 mM EDTA, and 1 mM DTT at 25 °C and either 50 or 100 mM KCl. Reaction rates were followed by the Malachite Green/ammonium molybdate assay for P_i formation for $AroA_{H6}$ in 50 mM KCl or by anion exchange TLC following conversion of [^{33}P]PEP to [^{33}P]phosphate for the other reactions, as described previously (*12*).

D313, which is from 1RF4 (D312 in *S. pneumoniae* AroA). The structures were very similar to each other, except for the D313A mutation in 1Q36 and movement of the E340 side chain (equivalent to E341 in *E. coli*) in 1RF4 in response to the electronegative fluorine atom in the F-THI. The active sites were superimposed using the residues D49, R100, R124, Q168, K340, R344, H385, R386 and the THI from 1Q36, and, for 1RF4, the residues D47, R96, R120, K339, R343, H384, R385 and the F-THI, except for the fluorine atom. The root-mean-squared difference in all atom positions was 0.7 Å. AroA-bound PEP was modeled into the same structure by superimposing the carboxylate and phosphate of PEP with the THI, while the EPSP model was built by superimposing the carboxylate and O5′ of the S3P moiety.

RESULTS

Kinetic Constants. Steady-state kinetic constants for wild-type recombinant *E. coli* AroA and AroA with a C-terminal His_6 tag, $AroA_{H6}$, were essentially identical (Table 1, Figure 3). Decreasing KCl from 100 to 50 mM increased k_{cat} and decreased K_M. Steady-state kinetic constants were determined for each mutant protein (Table 2, Figure 4), except $K_{M,PEP}$ could not be determined for K22A. The [PEP] versus v_0 profile was linear up to the highest [PEP] tested, 30 mM (data not shown), so only a lower limit could be estimated of $K_{M,PEP}$ >30 mM. The lack of curvature also meant that k_{cat} could not be determined, but $(k_{cat}/K_M)_{PEP}$ was 9 $M^{-1}\cdot s^{-1}$. Given the $(k_{cat}/K_M)_{PEP}$ value and $K_{M,PEP}$ >30 mM, the lower limit of k_{cat} would be >0.3 s^{-1}. Thus, the effect of the mutation on k_{cat} was <120-fold, and for $K_{M,PEP}$ it was >760-fold. The effect of the K22R mutation was smaller, 10-fold on k_{cat} and 60-fold on $K_{M,PEP}$.

Thermal Denaturation and Fluorescence Quenching. Thermal denaturation of $AroA_{H6}$ and mutants was irreversible, and the proteins precipitated. The range of apparent melting temperatures was small, from 59 °C for D313A to 63 °C for K22R, compared with 61 °C for $AroA_{H6}$.

Acrylamide quenching of Trp fluorescence was also used to probe protein stability and flexibility (*38*). Trp337 is in the protein core near the active site and is presumably the residue whose fluorescence decreases upon S3P binding (*12, 33*). Acrylamide quenches fluorescence if it makes contact with electronically excited Trp. The concentration dependence of quenching reflects the protein's flexibility in allowing acrylamide to diffuse into the protein core. Acrylamide quenching is reported as K_{SV}, with higher values indicating higher flexibility (*38*). K_{SV} was 5.1 M^{-1} for $AroA_{H6}$ and from 4.7 M^{-1} for D313A to 6.8 M^{-1} for E341Q (Table 2). Other proteins have shown >3-fold ranges in K_{SV} (*39*); therefore, the small range observed here again indicates that mutations had modest effects on AroA's active site.

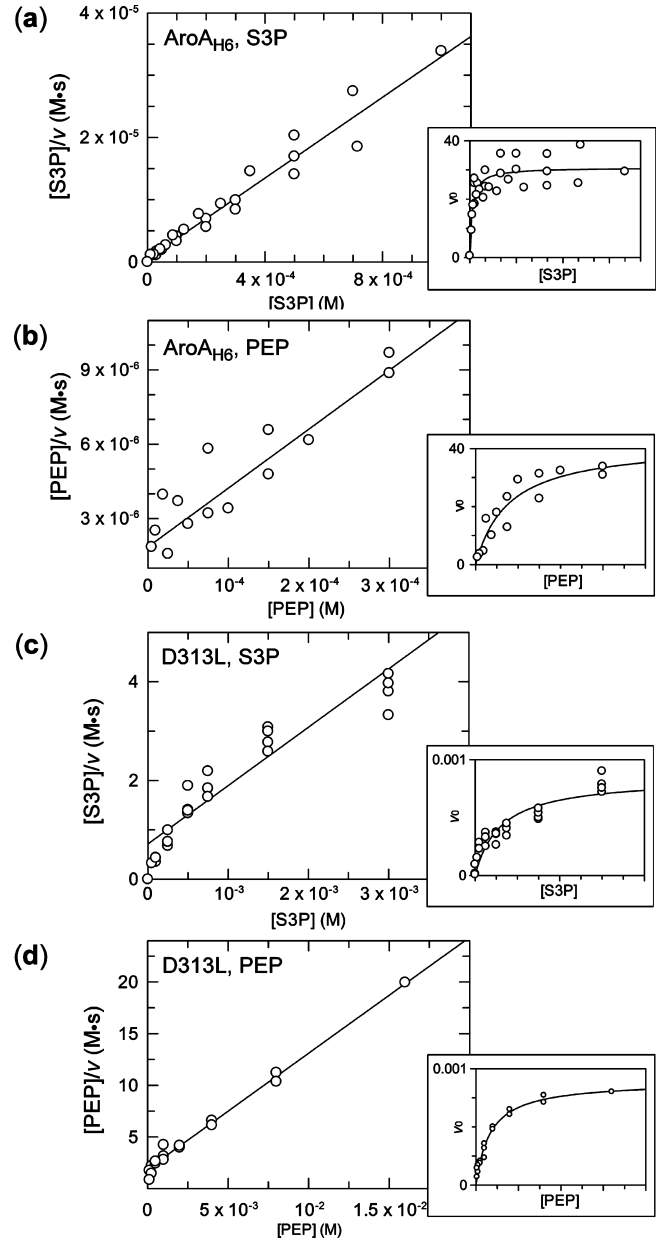

FIGURE 3: Steady-state kinetics for $AroA_{H6}$ and D313L, the mutant with the largest decrease in k_{cat}/K_M values, showing Hanes plots and (inset) v_0 versus [S]. (a) $AroA_{H6}$, variable S3P, (b) $AroA_{H6}$, variable PEP, (c) D313L, variable S3P, and (d) D313L, variable [PEP]. Rate data were fitted to eq 1 with k_{cat}, $K_{M,PEP}$, and $K_{M,S3P}$ all fitted simultaneously. Fixed substrate concentrations were [S3P] = 3 × 10^{-3} M and [PEP] = 8 × 10^{-3} M.

Presteady State Burst. One of the proposed mechanisms (Figure 2b) would predict a pre-steady-state burst of THI formation in the D313A mutant (see Discussion) (*22*). THI formation would be detected as P_i in the MG/AM colorimetric assay because the THI is unstable under the acidic

Table 2: Steady-State Kinetic Parameters and Stern−Volmer Constants for AroA Mutants[a,b]

$AroA_{H6}$ mutant	k_{cat} (s^{-1})	$(k_{cat}/K_M)_{S3P}$ ($M^{-1}\cdot s^{-1}$)	$(k_{cat}/K_M)_{PEP}$ ($M^{-1}\cdot s^{-1}$)	$K_{M,S3P}$ (M)	$K_{M,PEP}$ (M)	K_{SV} (M^{-1})
K22A[c]	>0.3	−	9 ± 2	2.0 (±0.7) × 10^{-3}	>0.03	5.1 ± 0.1
K22R	3.0 ± 0.2	1.6 (±0.2) × 10^{4}	1.2 (±0.2) × 10^{3}	1.9 (±0.3) × 10^{-4}	2.5 (±0.5) × 10^{-3}	6.0 ± 0.1
D313A	1.2 (±0.1) × 10^{-3}	6 ± 2	4 ± 1	2.1 (±0.7) × 10^{-4}	2.8 (±0.9) × 10^{-4}	4.7 ± 0.1
D313N	1.8 (±0.1) × 10^{-3}	9 ± 2	10 ± 2	2.0 (±0.6) × 10^{-4}	1.9 (±0.5) × 10^{-4}	5.5 ± 0.1
D313L	1.1 (±0.1) × 10^{-3}	1.6 ± 0.2	0.7 ± 0.1	7 (±1) × 10^{-4}	1.6 (±0.3) × 10^{-3}	5.8 ± 0.1
D313C	0.026 ± 0.003	68 ± 14	20 ± 4	4 (±1) × 10^{-4}	1.3 (±0.4) × 10^{-3}	6.3 ± 0.7
E341A[d]	4.2 (±0.4) × 10^{-4}	5 ± 2	9 ± 3	1.0 (±0.4) × 10^{-4}	5 (±2) × 10^{-5}	6.1 ± 0.2
E341Q	1.1 (±0.1) × 10^{-4}	27 ± 11	1.3 ± 0.5	4 (±2) × 10^{-5}	9 (±4) × 10^{-4}	6.8 ± 0.1
E341C[d]	3.6 (±0.2) × 10^{-3}	44 ± 11	21 ± 7	8 (±2) × 10^{-5}	1.7 (±0.6) × 10^{-4}	5.8 ± 0.1
E341M	1.7 (±0.1) × 10^{-3}	50 ± 13	0.9 ± 0.1	3.5 (±0.9) × 10^{-5}	1.9 (±0.3) × 10^{-3}	5.1 ± 0.3
H385A	0.41 ± 0.06	4 (±1) × 10^{3}	3 (±1) × 10^{2}	9 (±3) × 10^{-5}	1.5 (±0.7) × 10^{-3}	5.1 ± 0.1

[a] Reactions were as in Table 1 with 50 mM KCl and with P_i product detection with Malachite Green/ammonium molybdate. [b] Errors are the standard errors of the measured or fitted values. [c] $K_{M,PEP}$ was too high to measure. A plot of [PEP] vs v_0 was straight, up to the highest [PEP] tested, 30 mM, indicating that $K_{M,PEP}$ was >30 mM. As a result, only $(k_{cat}/K_M)_{PEP}$ could be determined. Because the kinetic constants for S3P and PEP are interrelated by eq 1, this means that k_{cat} and $(k_{cat}/K_M)_{S3P}$ also cannot be determined. $K_{M,S3P}$ was estimated from the one substrate Michaelis−Menten equation ($v_0 = k_{cat}[S][E]/([S] + K_M)$), ignoring [PEP]. Given $(k_{cat}/K_M)_{PEP} = 9\ M^{-1}\cdot s^{-1}$ and $K_{M,PEP}$ >0.03 M, it is possible to set a lower limit of k_{cat} >0.3 s^{-1}. [d] Given the small changes in K_M values for E341A and E341C, it is possible that the observed activity was due to contaminating wild-type AroA. Thus, the reported values of k_{cat} and k_{cat}/K_M would represent the upper limits of mutant activities, and they could be much lower.

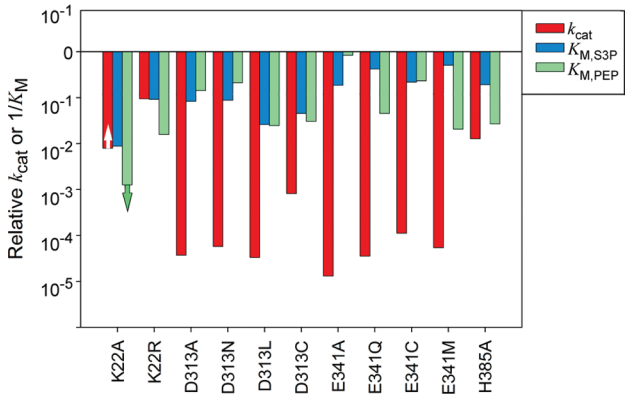

FIGURE 4: Catalytic impairment of mutations to K22, D313, E341, and H385. Values of k_{cat} and K_M are plotted relative to wild-type $AroA_{H6}$.

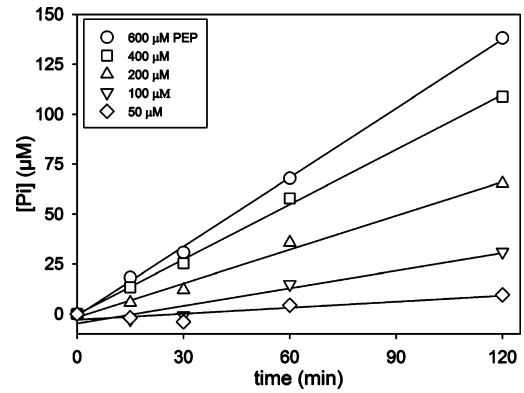

FIGURE 5: No pre-steady-state burst with D313A. The rate of P_i formation was measured with 20 μM D313A, 3 mM S3P, and varying PEP concentrations. THI would be detected as P_i formation, as it is unstable in the acidic MG/AM assay solution used to detect P_i, with $t_{1/2}$ ~1 s.

quenching conditions, breaking down to S3P, pyruvate, and P_i with $t_{1/2}$ ~1 s (*9*). No pre-steady-state burst was observed with D313A (Figure 5).

DISCUSSION

Catalytic Imperative. The exact catalytic roles of AroA active site residues have been elusive. Determining their function requires consideration of the reaction's catalytic imperative, that is, which parts of the reaction require the greatest transition-state stabilization. AroA activates the enolpyruvyl group to form either cationic intermediates or highly cationic transition states in the addition and elimination steps (*10, 11*). Protonating C3 of PEP or EPSP is highly unfavorable, requiring >15 kcal/mol (*40, 41*). Once a cation is formed, nucleophilic attack will be almost barrierless (*42*−*45*). Thus, in THI formation, the greater catalytic imperative is in protonating C3. In THI breakdown, forming the cationic intermediate will be the difficult step, with C−O bond cleavage potentially catalyzed by stabilizing the cationic center at C2 and by protonating O5′ for S3P departure or the bridging oxygen for P_i departure (*9, 20*). Deprotonating C3 of a cationic intermediate will be thermodynamically favorable (*41*) and kinetically facile (*40*), requiring little catalytic power.

The catalytic imperative for THI breakdown is smaller than for its formation, as shown by the rates of the corresponding nonenzymatic reactions. EPSP hydrolysis and THI breakdown both proceed through an EPSP cationic intermediate, but with rate constants of 7.7 × 10^{-8} s^{-1} (*10*) and 4.8 × 10^{-4} s^{-1} (*9*), respectively, at pH 7.5 and 25 °C. The 6200-fold difference in rate constants represents 5.2 kcal/mol higher activation energy for EPSP hydrolysis. PEP breakdown under these conditions occurs through P−O bond cleavage with a rate constant of 1 × 10^{-8} s^{-1} (*46*), meaning that C−O bond cleavage through C3 protonation is even more unfavorable. Thus, the catalytic imperative for forming the PEP cation is even higher than for the EPSP cation. The greater catalytic imperative in both the forward and reverse reactions is THI formation, rather than THI breakdown.

For wild-type AroA, the transition-state energies for each step are roughly equivalent, with the activation energy for PEP binding being slightly higher than for THI formation (*13*). Thus, AroA exerts its greatest catalytic power in THI formation, lowering the activation energy for the most chemically challenging step to below that for substrate binding.

Acid/Base Catalytic Residues. Based on THI partitioning experiments, we proposed previously that K22 was the general acid/base catalyst acting at O5′ and the phosphate oxygen, and that E341 was the general acid/base catalyst to protonate/deprotonate C3 (Figure 2a) (*12*). K22 is well located to interact with both the O5′H and phosphate oxygen atoms (Figure 6a).

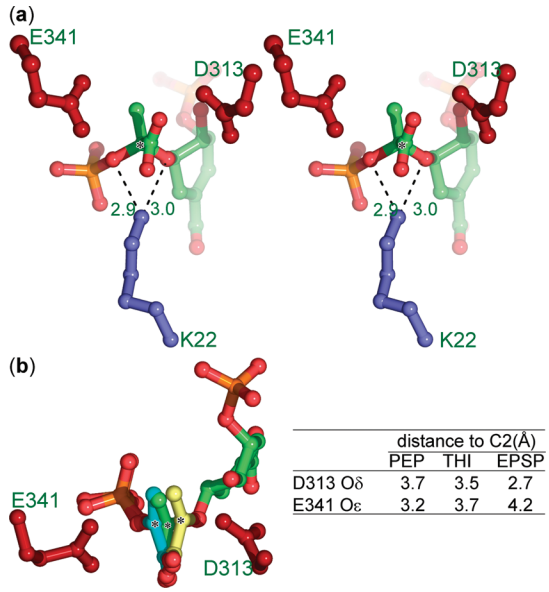

	distance to C2(Å)		
	PEP	THI	EPSP
D313 Oδ	3.7	3.5	2.7
E341 Oε	3.2	3.7	4.2

FIGURE 6: AroA·ligand interactions. C2 is indicated by an asterisk. (a) Interaction of K22 Nε (blue) with O5′ and phosphate oxygens of the THI (light-green). (b) C2 migration from PEP (cyan) to THI (green) to EPSP (yellow). The models of AroA with PEP, THI, and EPSP are described in the Experimental Procedures.

Both D313 and E341 were plausible candidate acid/base catalysts; however, numerous studies on the absolute and relative stereochemistries of AroA and MurA indicate *anti* addition with protonation on the *si* face of PEP (*14*−*19*), which would require that E341 be the acid catalyst.

Another recent mechanistic proposal was based on the AroA(D313A)·THI and MurA(D305A)·THI crystal structures (Figure 2b). K22 was proposed to both protonate C3 and deprotonate O5′H in the addition step, while D313 was proposed to be a base in the elimination step, using O4′H as a proton relay to deprotonate C3 (*22*). No general acid catalyst was identified for the elimination step. Several lines of evidence argue against this mechanism. It would create the opposite stereochemistry of that observed experimentally (*14*−*19*); K22 is poorly positioned to protonate C3 (Figure 6a), and THI partitioning experiments do not support this mechanism. With THI as the substrate, K22 mutations should have abolished S3P + PEP formation, while D313 mutations should have prevented EPSP + P_i formation. In both cases, there was no significant change in THI partitioning (*12*). A corollary to D313 being a general base catalyst and essential for P_i elimination is that THI would accumulate in the D313A mutant's active site, giving a pre-steady-state burst of THI formation (*22*). However, this was not observed for the D313A mutant (Figure 5). Thus, on the basis of the poor positioning of K22 to protonate C3, the incorrect stereochemistry, THI partitioning results, and the lack of a pre-steady-state burst in D313A, this mechanism does not account well for the observed behavior of AroA.

The observation of THI bound with AroA(D313A) in the crystal structure is not necessarily surprising. At equilibrium in solution, the species bound in the wild-type AroA active site are 4% {S3P + PEP}, 33% THI, and 61% {EPSP + P_i} (*1*). Thus, it would require only a modest shift in enzyme−substrate interaction energies to cause the THI to become the dominant species in the crystal.

Another proposed mechanism had E341 protonating C3 and D313 deprotonating O5′H in the addition step (*23*). In this proposal, phosphate promotes its own departure by deprotonating C3. Deprotonation of C3 by phosphate is in itself reasonable, but the overall mechanism does not match the THI partitioning results. The D313A and E341A mutations both caused >25 000-fold decreases in k_{cat}, which should have resulted in the THI partitioning completely forward to EPSP + P_i, which was not observed. Also, protonation of a nonbridging phosphate oxygen would not catalyze P_i departure; only protonation of the bridging oxygen will do so (*9*, *20*).

Lys22. The K22A mutation caused a >760-fold increase in $K_{M,PEP}$ and a >100-fold increase in $K_{M,S3P}$, indicating an important role in binding both substrates. The exact effect on k_{cat} is not known, but could be as much as 120-fold. K22 Nε is well located to interact with both O5′ and the phosphate bridging oxygen (Figure 6a). Although the effect on k_{cat} is modest compared to some acid/base catalytic residues, other cases of modest catalytic contributions are known (*48*, *49*). General base catalysis may not be important in THI formation because of the extreme reactivity of the presumed PEP cationic intermediate. Neutral O5′H would be able to attack without prior deprotonation, and, therefore, removing the base that deprotonates O5′H would have a relatively modest effect on catalysis.

In THI breakdown, both cationic intermediate stabilization and general acid catalysis may contribute to catalysis. General acid catalysis by K22 would activate the O5′H and P_i leaving groups for departure, and, indeed, this may account for the observed effect on k_{cat} upon mutation. The smaller activation energy for THI breakdown than formation and the catalytic effect of electrostatic stabilization of the cationic intermediates may combine to decrease the need for general acid catalysis in the elimination step.

The K22R mutation had only a 10-fold effect on k_{cat}, presumably reflecting electrostatic stabilization of the anionic leaving groups in THI breakdown or possibly general acid catalysis by the guanidinium group. Arg is generally a poor general acid catalyst, with an unperturbed pK_a = 12.5. However, that is lower than S3P's O5′H (pK_a ~17) and similar to PO_4^{3-} (pK_a ~12.3), and the Arg side chain in K22R is located in an environment that lowers the Lys pK_a by 3 pH units (*21*), so general acid catalysis, though unlikely, cannot be completely ruled out.

Carboxylate Mutations. Mutations to both D313 and E341 caused large decreases in k_{cat} and small increases in K_M, which indicates that both residues are crucial to catalysis.

Asp313. D313 mutations decreased k_{cat} up to 30 000-fold, but increased K_M values no more than 40-fold. Neither Asn, which is isosteric and polar, nor Leu, which is roughly isosteric and nonpolar, could replace Asp. The k_{cat} effect on D313C was smaller, 1200-fold. Cys is ionizable and could potentially act as an acid/base catalyst, or the thiolate form could stabilize cationic intermediates electrostatically. At pH 7.5, Cys would be 16% in the anion form assuming an unperturbed pK_a = 8.3. This would account for the higher catalytic activity for D313C than for D313A.

Glu341. E341 mutations decreased k_{cat} up to 76 000-fold, while K_M values increased by less than 20-fold. None of the other side chains tested significantly rescued the E341A mutation, including Gln which is isosteric and polar, Met

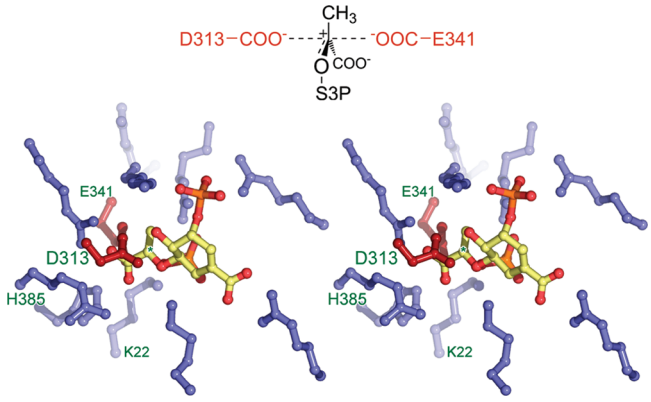

FIGURE 7: Electrostatic sandwich in (top) cartoon and stereo representations (bottom) of the EPSP cation model. C2 is indicated by an asterisk. PEP and EPSP are good models for the structures of the corresponding cations; the C2−C3 bonds lengthen by ~0.3 Å and the C2−O5/C2−O2 bonds shorten by ~0.3 Å in the cation forms, but the overall geometry is essentially identical.

which is roughly isosteric and nonpolar, and Cys which is ionizable but has a shorter side chain than Glu. The effects on $K_{M,S3P}$ were modest, 2- to 5-fold. The effects on $K_{M,PEP}$ with the shorter side chain mutants were also modest, 1.2-fold for E341A and 4-fold for E341C. This implies little or no direct interaction between E341 and the substrate PEP. The effects on $K_{M,PEP}$ were larger for the other mutants, 22-fold for E341Q and 49-fold for E341M. This indicates some unfavorable interactions with PEP, possibly as a consequence of changes in the side chain conformation. The effect of the H385A mutation is consistent with that interpretation. H385 is positioned to form a 2.7 Å hydrogen bond with E341 and to orient the carboxylate group. It had a 37-fold effect on $K_{M,PEP}$, similar to E341Q and E341M, even though it does not make direct contact with the substrates.

In some proposed mechanisms, including ours, E341 acts as an acid/base catalyst, while it has no specific role in other proposals. E341 is positioned in most crystal structures to both act as an acid/base catalyst and stabilize cationic intermediates (Figure 6b,7), though in the AroA·F-THI crystal structure it moves away from the electronegative fluorine atom of the F-THI (*24*).

Electrostatic Sandwich. D313 and E341 are positioned on either side of the positive charge in the proposed cationic intermediates, forming an "electrostatic sandwich" (Figure 7). With the EPSP cation, the P_i product may also be positioned to form part of the electrostatic sandwich (Figure 7). AroA's active site consists of many cationic side chains and a small number of carboxylate side chains. Binding S3P (charge = −3) and PEP (charge = −3) in the active site requires overcoming significant electrostatic repulsion to bring the negative charges into close proximity. The effect of ionic strength is consistent with most enzyme−substrate contacts being ionic; decreasing KCl from 100 mM to 50 mM increased k_{cat} 2.4-fold and decreased K_M ~5-fold (Table 1). Lower ionic strength decreases dielectric screening and increases the strength of electrostatic interactions, tightening substrate binding and increasing charge stabilization in the cationic intermediates.

The D313 and E341 carboxylate groups bracket the putative cationic center (Figure 7). D313 and E341 are conspicuously outnumbered by the surrounding cationic side chains in the active site, but well located to stabilize a positive charge at C2. As the enolpyruvyl group is transformed from PEP to the THI and then to EPSP, C2 migrates by ~1 Å. In all these structures, both carboxylate residues are close enough to stabilize a charge at C2, particularly given the $1/r$ distance dependence that makes electrostatic interactions effective over longer distances than hydrogen bonding or van der Waals interactions. The observed distances are based on a rigid active site; however, AroA crystal structures show domain-scale motions upon ligand binding, plus conformational changes in the loop containing E341 (*24, 50*−*52*) and E341 side chain movements (*24, 53*). Trp fluorescence changes upon ligand binding also point toward conformation changes (*33, 54, 55*), as do hydrogen−deuterium exchange studies (*56*). Thus, while the observed C2···carboxylate distances are already reasonable, it is likely that further conformational changes would occur during catalysis to optimize these interactions.

The departing P_i product may also stabilize the EPSP cation electrostatically. P_i increases catalysis 10^5-fold in the reverse reaction, as determined from the k_{cat} values for AroA-catalyzed EPSP hydrolysis versus the normal reverse reaction of EPSP + P_i to S3P and PEP (*10, 54*), though its exact electrostatic contribution would be difficult to distinguish from the conformational change induced upon P_i binding (*54*) or differences in transition state structure.

Electrostatic stabilization by D313 is consistent with the fact that neither the Asn nor Leu mutants rescued D313A's activity, but that Cys showed a slight improvement relative to Ala. Cys is ionizable, and, although the sulfur atom of the thiolate form would be further from C2 than Asp Oδ, it could potentially stabilize the cationic center. If D313 is providing electrostatic stabilization, then the equivalent residue in MurA, D305, would be expected to play the same catalytic role. This is supported by the MurA(C115S)·EP-UDPGlcNAc·P_i crystal structure, where D305 Oδ was positioned 3.1 Å from C2 (*47*). This structure is also consistent with a role for P_i in an electrostatic sandwich, which has a C2···O distance of 3.3 Å. There is no strict counterpart for E341 in MurA; C115 was previously proposed as a general acid/base catalyst that would play the same role as E341 (*57*), but more recent evidence suggests a role in product dissociation (*47*).

CONCLUSIONS

Previous studies on AroA's mechanism, including our own (*12*), have tended to focus on acid/base catalytic residues. However, the large catalytic imperative to activate the enolpyruvyl group to form a cation intermediate or cationic transition states, and the large catalytic roles for D313 and E341, point to electrostatic stabilization of positive charge at C2 as an important catalytic strategy. The experimental evidence is also consistent with our previous proposal that E341 is an acid/base catalytic residue that protonates C3 in the addition step and deprotonates it in the elimination step. Thus, we propose a dual acid/base and electrostatic catalysis role for E341. The largest effect of the K22A mutation was on substrate binding, particularly PEP. The effect on catalysis, as reflected by k_{cat}, was perhaps smaller than expected; however, a consideration of the catalytic imperative for THI formation suggests that a general base catalyst at that step may not be crucial.

ACKNOWLEDGMENT

We thank Mark Maraschiello for performing some of the fluorescence titrations and melting temperature measurements reported here, Jennifer Wright for determining the steady-state kinetic parameters for wild-type AroA, and Grace Lou for her helpful comments on the manuscript.

REFERENCES

1. Anderson, K. S., and Johnson, K. A. (1990) Kinetic and structural analysis of enzyme intermediates: Lessons from EPSP synthase. *Chem. Rev. 90*, 1131–1149.
2. Roberts, F., Roberts, C. W., Johnson, J. J., Kyle, D. E., Krell, T., Coggins, J. R., Coombs, G. H., Milhous, W. K., Tzipori, S., Ferguson, D. J., Chakrabarti, D., and McLeod, R. (1998) Evidence for the shikimate pathway in apicomplexan parasites. *Nature 393*, 801–805.
3. Priebe, G. P., Meluleni, G. J., Coleman, F. T., Goldberg, J. B., and Pier, G. B. (2003) Protection against fatal Pseudomonas aeruginosa pneumonia in mice after nasal immunization with a live, attenuated aroA deletion mutant. *Infect. Immun. 71*, 1453–1461.
4. Stritzker, J., Janda, J., Schoen, C., Taupp, M., Pilgrim, S., Gentschev, I., Schreier, P., Geginat, G., and Goebel, W. (2004) Growth, virulence, and immunogenicity of Listeria monocytogenes aro mutants. *Infect. Immun. 72*, 5622–5629.
5. Steinrucken, H. C., and Amrhein, N. (1980) The herbicide glyphosate is a potent inhibitor of 5-enolpyruvyl-shikimic acid-3-phosphate synthase. *Biochem. Biophys. Res. Commun. 94*, 1207–1212.
6. Kahan, F. M., Kahan, J. S., Cassidy, P. J., and Kropp, H. (1974) Mechanism of action of fosfomycin (phosphonomycin). *Ann. N.Y. Acad. Sci. 235*, 364–386.
7. Anderson, K. S., Sikorski, J. A., Benesi, A. J., and Johnson, K. A. (1988) Isolation and structural elucidation of the tetrahedral intermediate in the EPSP synthase enzymic pathway. *J. Am. Chem. Soc. 110*, 6577–6579.
8. Marquardt, J. L., Brown, E. D., Walsh, C. T., and Anderson, K. S. (1993) Isolation and structural elucidation of a tetrahedral intermediate in the UDP-*N*-acetylglucoamine enolpyruvyl transferase enzymatic pathway. *J. Am. Chem. Soc. 115*, 10398–10399.
9. Byczynski, B., Mizyed, S., and Berti, P. J. (2003) Nonenzymatic breakdown of the tetrahedral (α-carboxyketal phosphate) intermediates of MurA and AroA, two carboxyvinyl transferases. Protonation of different functional groups controls the rate and fate of breakdown. *J. Am. Chem. Soc. 125*, 12541–12550.
10. Clark, M. E., and Berti, P. J. (2007) Enolpyruvyl Activation by Enolpyruvylshikimate-3-phosphate Synthase. *Biochemistry 46*, 1933–1940.
11. Anton, D. L., Hedstrom, L., Fish, S., and Abeles, R. H. (1983) Mechanism of enolpyruvylshikimate-3-phosphate synthase exchange of phosphoenolpyruvate with solvent protons. *Biochemistry 22*, 5903–5908.
12. Mizyed, S., Wright, J. E. I., Byczynski, B., and Berti, P. J. (2003) Identification of the catalytic residues of AroA (enolpyruvylshikimate 3-phosphate synthase) using partitioning analysis. *Biochemistry 42*, 6986–6995.
13. Anderson, K. S., Sikorski, J. A., and Johnson, K. A. (1988) A tetrahedral intermediate in the EPSP synthase reaction observed by rapid quench kinetics. *Biochemistry 27*, 7395–7406.
14. Grimshaw, C. E., Sogo, S. G., Copley, S. D., and Knowles, J. R. (1984) Synthesis of stereoselectively labeled [9-^{2}H,^{3}H]chorismate and the stereochemical course of 5-enolpyruvoylshikimate-3-phosphate synthetase. *J. Am. Chem. Soc. 106*, 2699–2700.
15. Lee, J. J., Asano, Y., Shieh, T.-L., Spreafico, F., Lee, K., and Floss, H. G. (1984) Steric course of the 5-enolpyruvylshikimate-3-phosphate synthetase and anthranilate synthetase reactions. *J. Am. Chem. Soc. 106*, 3367–3368.
16. Kim, D. H., Tucker-Kellogg, G. W., Lees, W. J., and Walsh, C. T. (1996) Analysis of fluoromethyl group chirality establishes a common stereochemical course for the enolpyruvyl transfers catalyzed by EPSP synthase and UDP-GlcNAc enolpyruvyl transferase. *Biochemistry 35*, 5435–5440.
17. Skarzynski, T., Kim, D. H., Lees, W. J., Walsh, C. T., and Duncan, K. (1998) Stereochemical course of enzymatic enolpyruvyl transfer and catalytic conformation of the active site revealed by the crystal structure of the fluorinated analogue of the reaction tetrahedral intermediate bound to the active site of the C115A mutant of MurA. *Biochemistry 37*, 2572–2577.
18. Kim, D. H., Lees, W. J., and Walsh, C. T. (1995) Stereochemical analysis of the tetrahedral adduct formed at the active site of UDP-GlcNAc enolpyruvyl transferase from the pseudosubstrates, (E)- and (Z)-3-fluorophosphoenolpyruvate, in D_2O. *J. Am. Chem. Soc. 117*, 6380–6381.
19. Lees, W. J., and Walsh, C. T. (1995) Analysis of the enol ether transfer catalyzed by UDP-GlcNAc enolpyruvyl transferase using (*E*)- and (*Z*)-isomers of phosphoenolbutyrate: Stereochemical, partitioning, and isotope effect studies. *J. Am. Chem. Soc. 117*, 7329–7337.
20. Loncke, P. G., and Berti, P. J. (2006) Implications of Protonation and Substituent Effects for C-O and O-P Bond Cleavage in Phosphate Monoesters. *J. Am. Chem. Soc. 128*, 6132–6140.
21. Huynh, Q. K., Kishore, G. M., and Bild, G. S. (1988) 5-Enolpyruvyl shikimate 3-phosphate synthase from Escherichia coli. Identification of Lys-22 as a potential active site residue. *J. Biol. Chem. 263*, 735–739.
22. Eschenburg, S., Kabsch, W., Healy, M. L., and Schonbrunn, E. (2003) A new view of the mechanisms of UDP-*N*-acetylglucosamine enolpyruvyl transferase (MurA) and 5-enolpyruvylshikimate-3-phosphate synthase (AroA) derived from x-ray structures of their tetrahedral reaction intermediate states. *J. Biol. Chem. 278*, 49215–49222.
23. An, M., Maitra, U., Neidlein, U., and Bartlett, P. A. (2003) 5-Enolpyruvylshikimate 3-phosphate synthase: Chemical synthesis of the tetrahedral intermediate and assignment of the stereochemical course of the enzymatic reaction. *J. Am. Chem. Soc. 125*, 12759–12767.
24. Park, H., Hilsenbeck, J. L., Kim, H. J., Shuttleworth, W. A., Park, Y. H., Evans, J. N. S., and Kang, C. (2004) Structural studies of Streptococcus pneumoniae EPSP synthase in unliganded state, tetrahedral intermediate-bound state and S3P-GLP-bound state. *Mol. Microbiol. 51*, 963–971.
25. Shuttleworth, W. A., Pohl, M. E., Helms, G. L., Jakeman, G. L., and Evans, J. N. S. (1999) Site-directed mutagenesis of putative active site residues of 5-enolpyruvylshikimate-3-phosphate synthase. *Biochemistry 38*, 296–302.
26. Huynh, Q. K., Bauer, S. C., Bild, G. S., Kishore, G. M., and Borgmeyer, J. R. (1988) Site-directed mutagenesis of Petunia hybrida 5-enolpyruvylshikimate-3- phosphate synthase: Lys-23 is essential for substrate binding. *J. Biol. Chem. 263*, 11636–11639.
27. Padgette, S. R., Re, D. B., Gasser, C. S., Eichholtz, D. A., Frazier, R. B., Hironaka, C. M., Levine, E. B., Shah, D. M., Fraley, R. T., and Kishore, G. M. (1991) Site-directed mutagenesis of a conserved region of the 5-enolpyruvylshikimate-3-phosphate synthase active site. *J. Biol. Chem. 266*, 22364–22369.
28. Shuttleworth, W. A., and Evans, J. N. S. (1994) Site-directed mutagenesis and NMR studies of histidine 385 mutants of 5-enolpyruvylshikimate-3-phosphate (EPSP) synthase. *Biochemistry 33*, 7062–7068.
29. Shuttleworth, W. A., and Evans, J. N. S. (1996) The H385N mutant of 5-enolpyruvylshikimate-3-phosphate synthase: kinetics, fluorescence, and nuclear magnetic resonance studies. *Arch. Biochem. Biophys. 334*, 37–42.
30. Samland, A. K., Amrhein, N., and Macheroux, P. (1999) Lysine 22 in UDP-N-acetylglucosamine enolpyruvyl transferase from *Enterobacter cloacae* is crucial for enzymatic activity and the formation of covalent adducts with the substrate phosphoenolpyruvate and the antibiotic fosfomycin. *Biochemistry 38*, 13162–13169.
31. Eschenburg, S., Healy, M. L., Priestman, M. A., Lushington, G. H., and Schonbrunn, E. (2002) How the mutation glycine96 to alanine confers glyphosate insensitivity to 5-enolpyruvyl shikimate-3-phosphate synthase from *Escherichia coli*. *Planta 216*, 129–135.
32. He, M., Nie, Y.-F., and Xu, P. (2003) A T42M substitution in bacterial 5-enolpyruvylshikimate-3-phosphate synthase (EPSPS) generates enzymes with increased resistance to glyphosate. *Biosci., Biotechnol., Biochem. 67*, 1405–1409.
33. Anderson, K. S., Sikorski, J. A., and Johnson, K. A. (1988) Evaluation of 5-enolpyruvoylshikimate-3-phosphate synthase substrate and inhibitor binding by stopped-flow and equilibrium fluorescence measurements. *Biochemistry 27*, 1604–1610.
34. Lanzetta, P. A., Alvarez, L. J., Reinach, P. S., and Candia, O. A. (1979) An improved assay for nanomole amounts of inorganic phosphate. *Anal. Biochem. 100*, 95–97.

35. Hess, H. H., and Derr, J. E. (1975) Assay of inorganic and organic phosphorus in the 0.1−5 nanomole range. *Anal. Biochem. 63*, 607–613.
36. Gruys, K. J., Marzabadi, M. R., Pansegrau, P. D., and Sikorski, J. A. (1993) Steady-state kinetic evaluation of the reverse reaction for *Escherichia coli* 5-enolpyruvoylshikimate-3-phosphate synthase. *Arch. Biochem. Biophys. 304*, 345–351.
37. Gruys, K. J., Walker, M. C., and Sikorski, J. A. (1992) Substrate synergism and the steady-state kinetic reaction mechanism for EPSP synthase from *Escherichia coli*. *Biochemistry 31*, 5534–5544.
38. Eftink, M. R., and Ghiron, C. A. (1976) Exposure of tryptophanyl residues in proteins. Quantitative determination by fluorescence quenching studies. *Biochemistry 15*, 672–680.
39. Tang, L., van Merode, A. E., Lutje Spelberg, J. H., Fraaije, M. W., and Janssen, D. B. (2003) Steady-state kinetics and tryptophan fluorescence properties of halohydrin dehalogenase from *Agrobacterium radiobacter*. Roles of W139 and W249 in the active site and halide-induced conformational change. *Biochemistry 42*, 14057–14065.
40. Kresge, A. J., Sagatys, D. S., and Chen, H. L. (1977) Vinyl ether hydrolysis 0.9. Isotope effects on proton-transfer from hydronium ion. *J. Am. Chem. Soc. 99*, 7228–7233.
41. Kresge, A. J., Leibovitch, M., and Sikorski, J. A. (1992) Acid-catalyzed hydrolysis of 5-enolpyruvylshikimate 3-phosphate (EPSP) and some simple models of its vinyl ether functional group. *J. Am. Chem. Soc. 114*, 2618–2622.
42. Richard, J. P., Williams, K. B., and Amyes, T. L. (1999) Intrinsic barriers for the reactions of an oxocarbenium ion in water. *J. Am. Chem. Soc. 121*, 8403–8404.
43. Richard, J. P. (1995) A consideration of the barrier for carbocation-nucleophile combination reactions. *Tetrahedron 51*, 1535–1573.
44. Horenstein, B. A., and Bruner, M. (1998) The *N*-acetyl neuraminyl oxocarbenium ion is an intermediate in the presence of anionic nucleophiles. *J. Am. Chem. Soc. 120*, 1357–1362.
45. McCann, J. A. B., and Berti, P. J. (2007) Transition state analysis of acid-catalyzed dAMP hydrolysis. *J. Am. Chem. Soc. 129*, 7055–7064.
46. Benkovic, S. J., and Schray, K. J. (1968) The kinetics and mechanisms of phosphoenolpyruvate hydrolysis. *Biochemistry 7*, 4090–4096.
47. Eschenburg, S., Priestman, M., and Schonbrunn, E. (2005) Evidence that the fosfomycin target Cys115 in UDP-N-acetylglucosamine enolpyruvyl transferase (MurA) is essential for product release. *J. Biol. Chem. 280*, 3757–3763.
48. Denu, J. M., Zhou, G., Guo, Y., and Dixon, J. E. (1995) The catalytic role of aspartic acid-92 in a human dual-specific protein-tyrosine-phosphatase. *Biochemistry 34*, 3396–3403.
49. Frandsen, T. P., Dupont, C., Lehmbeck, J., Stoffer, B., Sierks, M. R., Honzatko, R. B., and Svensson, B. (1994) Site-directed mutagenesis of the catalytic base glutamic acid 400 in glucoamylase from *Aspergillus niger* and of tyrosine 48 and glutamine 401, both hydrogen-bonded to the gamma-carboxylate group of glutamic acid 400. *Biochemistry 33*, 13808–13816.
50. Stallings, W. C., Abdel-Meguid, S. S., Lim, L. W., Shieh, H.-S., Dayringer, H. E., Leimgruber, N. K., Stegeman, R. A., Anderson, K. S., Sikorski, J. A., Padgette, S. R., and Kishore, G. H. (1991) Structure and topological symmetry of the glyphosate target 5-enolpyruvylshikimate-3-phosphate synthase: A distinctive protein fold. *Proc. Natl. Acad. Sci. U.S.A. 88*, 5046–5050.
51. Schonbrunn, E., Eschenburg, S., Shuttleworth, W. E., Schloss, J. V., Amrhein, N., Evans, J. N. S., and Kabsch, W. (2001) Interaction of the herbicide glyphosate with its target enzyme 5-enolpyruvylshikimate 3-phosphate synthase in atomic detail. *Proc. Natl. Acad. Sci. U.S.A. 98*, 1376–1380.
52. Funke, T., Healy-Fried, M. L., Han, H., Alberg, D. G., Bartlett, P. A., and Schonbrunn, E. (2007) Differential Inhibition of Class I and Class II 5-Enolpyruvylshikimate-3-phosphate Synthases by Tetrahedral Reaction Intermediate Analogues. *Biochemistry 46*, 13344–13351.
53. Priestman, M. A., Healy, M. L., Becker, A., Alberg, D. G., Bartlett, P. A., Lushington, G. H., and Schonbrunn, E. (2005) Interaction of phosphonate analogues of the tetrahedral reaction intermediate with 5-enolpyruvylshikimate-3-phosphate synthase in atomic detail. *Biochemistry 44*, 3241–3248.
54. Zhang, F., and Berti, P. J. (2006) Phosphate analogues as probes of the catalytic mechanisms of MurA and AroA, two carboxyvinyl transferases. *Biochemistry 45*, 6027–6037.
55. Sammons, R. D., Gruys, K. J., Anderson, K. S., Johnson, K. A., and Sikorski, J. A. (1995) Reevaluating glyphosate as a transition-state inhibitor of EPSP synthase: identification of an EPSP synthase.EPSP.glyphosate ternary complex. *Biochemistry 34*, 6433–6440.
56. Marques, M. R., Vaso, A., Neto, J. R., Fossey, M. A., Oliveira, J. S., Basso, L. A., dos Santos, D. S., de Azevedo Junior, W. F., and Palma, M. S. (2008) Dynamics of Glyphosate-Induced Conformational Changes of *Mycobacterium tuberculosis* 5-Enolpyruvylshikimate-3-phosphate Synthase (EC 2.5.1.19) Determined by Hydrogen-Deuterium Exchange and Electrospray Mass Spectrometry. *Biochemistry 47*, 7509–7522.
57. Kim, D. H., Lees, W. J., Kempsell, K. E., Lane, W. S., Duncan, K., and Walsh, C. T. (1996) Characterization of a Cys115 to Asp substitution in the *Escherichia coli* cell wall biosynthetic enzyme UDP-GlcNAc enolpyruvyl transferase (MurA) that confers resistance to inactivation by the antibiotic fosfomycin. *Biochemistry 35*, 4923–4928.

BI802251S